

# Normal-incidence efficiencies of multilayer-coated laminar gratings for the Extreme-Ultraviolet Imaging Spectrometer on the Solar-B mission

John F. Seely, Charles M. Brown, David L. Windt, Soizik Donguy, and Benjawan Kjornrattanawanich

The normal-incidence efficiencies of two laminar gratings and the reflectances of two parabolic mirrors with matching multilayer coatings were measured by monochromatic synchrotron radiation and were compared with modeling calculations. These optics were developed for the Extreme-Ultraviolet Imaging Spectrometer to be launched on the Japanese Solar-B mission. Each optic has two sectors coated with Mo/Si multilayers that reflect the 17–21-nm and 25–29-nm wave bands at normal incidence. The measured peak grating efficiencies are in the 8%–12% range and are in good agreement with efficiency calculations that account for the effects of groove profile and the microroughness as determined by atomic force microscopy. © 2004 Optical Society of America

OCIS codes: 050.1950, 310.1620.

## 1. Introduction

The application of a high-reflectance multilayer coating greatly enhances the normal-incidence efficiency of a diffraction grating in the extreme-ultraviolet (EUV) wavelength region. The period of the multilayer coating and the groove profile of the underlying grating are optimized so that the coating has high reflectance and the grooves have high diffraction efficiency in a selected wavelength range. Gratings with laminar (ideally rectangular) and blazed (triangular) groove profiles and with matched multilayer coatings have been demonstrated to have relatively high normal-incidence efficiencies in the 9–40-nm wavelength range (see the review in Ref. 1 and references therein). In addition, the efficiencies measured by synchrotron radiation are in good agreement with the efficiencies calculated with the modified integral formalism and accounting for the

groove profile and microroughness as determined by atomic force microscopy (AFM).<sup>2</sup> The experimental and computational techniques have matured to the extent that, in general, gratings and matching multilayer coatings can be designed and fabricated with predictable and reliable performance in the EUV wavelength region provided that accurate optical constants are available for the specific materials and wavelengths of interest. This has led to the selection of a multilayer-coated grating for the Extreme-Ultraviolet Imaging Spectrometer (EIS) on the Solar-B mission, the first implementation of a multilayer grating on a satellite instrument.<sup>3</sup> We describe here the performance of two flight gratings and two flight mirrors that have optimized groove profiles and matching multilayer coatings developed for the EIS instrument.

The EIS instrument was designed by an international collaboration of scientists and engineers in the United States, Japan, and Britain. This instrument utilizes an off-axis parabolic telescope mirror and a toroidal diffraction grating, both operating near normal incidence with high-reflectance Mo/Si multilayer coatings.<sup>4</sup> Normal-incidence optics are utilized to ensure good image quality, and only two reflections are required, maintaining high instrument sensitivity in the EUV. Mo/Si multilayers with different periods cover each half of the mirror and grating. The multilayer coatings have high normal-incidence reflectance in two wavelength regions, 17–21 and 25–29 nm, which include many intense solar spectral

---

J. F. Seely (john.seely@nrl.navy.mil) and C. M. Brown are with the Space Science Division, U.S. Naval Research Laboratory, Code 7674, 4555 Overlook Avenue, SW, Washington, D.C. 20375. D. L. Windt and S. Donguy are with the Astrophysics Laboratory, Columbia University, 550 West 120th Street, New York, New York 10027. B. Kjornrattanawanich is with the National Synchrotron Light Source, Universities Space Research Association, Upton, New York 11973.

Received 31 August 2003; revised manuscript received 4 November 2003; accepted 20 November 2003.

0003-6935/04/071463-09\$15.00/0

© 2004 Optical Society of America

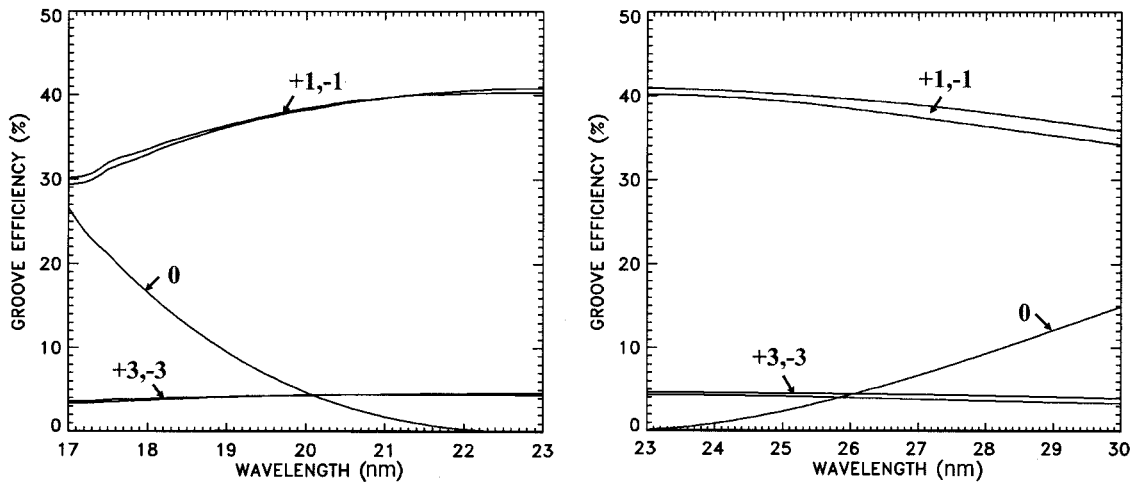


Fig. 1. Calculated groove efficiency of the baseline EIS grating substrate with a 5.8-nm groove depth.

lines that are emitted over a wide range of plasma temperature. The baseline multilayer coatings specified for the EIS instrument have peak reflectances of 32% and 23% at wavelengths of 19.5 and 26.8 nm, respectively, and this results in high instrument throughput in the two wave bands.

The mirrors are superpolished off-axis parabolas with a focal length of 1939 mm and a figure accuracy better than  $\lambda/25$ . They were fabricated from Zerodur material by Tinsley Laboratories, Inc. The grating blanks, fabricated by Zeiss Laser Optics GmbH, are of fused silica and have toroidal radii of 1182.9 mm in the dispersion direction and 1178.3 mm in the perpendicular direction. The slope error in the figure is 0.49 arc sec rms, and the microroughness of the blank is  $<0.25$  nm rms. The mirror produces a solar image at the slit of the EIS spectrometer. The toroidal grating is used at a magnification of 1.44 and forms stigmatic images of the slit plane on two CCD detectors for the bandpasses centered at 19.5- and 27.0-nm wavelengths. The diameter of the grating blank is 100 mm, and the usable patterned area is specified to have a 90-mm diameter. The diameter of the mirror blank is 160 mm with a usable diameter of 150 mm.

## 2. Grating Substrates and Predicted Efficiencies

The EUV capabilities of the EIS multilayer optics were designed and optimized with computer codes that model the reflectance of the multilayer coating and the efficiency of the multilayer grating.<sup>3</sup> The grating efficiency was calculated with the PCGRATE code that was developed and validated by Goray and Seely.<sup>2,5</sup> This code implements the modified integral approach to solve the boundary-value problem of electromagnetic radiation incident on a diffraction grating with a multilayer coating. The code accounts for the thicknesses and optical properties of the layers and the two polarization components of the incident radiation. The computational model makes direct use of the measured groove profile as deter-

mined by AFM, thereby accurately accounting for the groove shape and microroughness.

To a first approximation, the overall efficiency of the multilayer-coated grating is the product of the grating groove efficiency and the reflectance of the multilayer coating. Experimentally, the groove efficiency is derived from the ratio of the measured efficiency of the multilayer-coated grating and the reflectance of a flat mirror with the same multilayer coating as the grating. In general, for a selected wavelength operating near normal incidence, the optimal laminar groove profile has a groove depth equal to one fourth the operating wavelength and equal groove and land widths. Then the first orders have maximal groove efficiencies, the higher odd orders ( $>1$ ) have low efficiencies, the zero order is minimal, and the even orders have negligible efficiencies. The EIS grating substrates were specified to have 4200 grooves/mm, a laminar groove profile with a depth of 5.8 nm, and  $<0.5$ -nm microroughness. In the EIS instrument, the angles of incidence at the centers of the short-band and long-band sides of the grating are  $4.268^\circ$  and  $4.690^\circ$ , respectively. Because polarization effects are small near normal incidence, the efficiencies are presented for the case of unpolarized incidence radiation.

The calculated groove efficiencies in the two wave bands are shown in Fig. 1. The 5.8-nm groove depth results in a first-order peak groove efficiency at a wavelength of 23 nm that is midway between the two EIS wave bands (17–21 and 25–29 nm). The predicted peak value of the first-order groove efficiency is 41% at a 23-nm wavelength, and the groove efficiency decreases to approximately 30–35% at the two extreme ends of the EIS wave bands at 17 and 29 nm. The groove efficiencies in the higher orders ( $>1$ ) are  $<5\%$ . The groove profile was assumed to have sloping sides with an angle of  $35^\circ$  as indicated by AFM studies of a Zeiss test grating.

Because the groove efficiency is a rather weak function of wavelength and angle of incidence near nor-

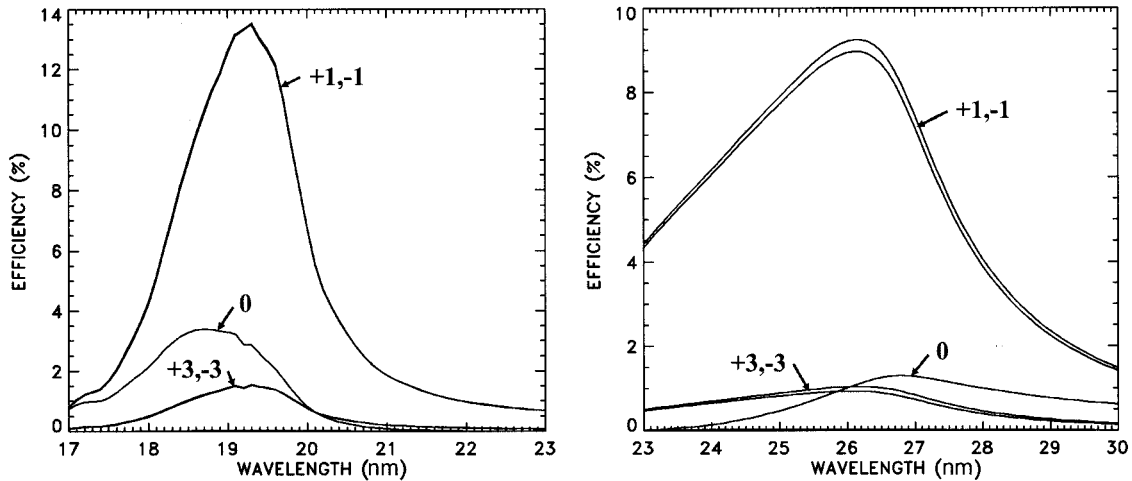


Fig. 2. Calculated efficiency of the EIS grating with the two baseline multilayer coatings.

mal, it is possible to use one groove frequency uniformly across the entire grating surface and to utilize different multilayer coatings on each half of the grating to reflect the two EIS wave bands. Thus half of the grating is coated to reflect the 17–21-nm wave band and the other half the 25–29-nm wave band. The corresponding halves of the parabolic mirror are coated with the same multilayers. In the EIS instrument, the angles of incidence are  $2.70^\circ$  and  $1.59^\circ$  at the centers of the short-band and long-band sides of the mirror, respectively.

The multilayer reflectance profiles are narrower in wavelength than the groove efficiency profile, and the product of the mirror and grating reflectance profiles primarily determines the two usable wavelength ranges of the EIS spectrometer. The peak reflectance values and the widths of the reflectance profiles are the most important factors in the determination of the wavelength-dependent throughput of the EIS spectrometer in the two wave bands.

We performed detailed computer simulations of the multilayer-coated grating, based on the specified groove profile and accounting for the expected micro-roughness of the grating substrate and nonideal Mo/Si multilayer interfaces, during the design phase of the EIS instrument.<sup>3</sup> Figure 2 illustrates the two efficiency bandpasses that are primarily determined

by the reflectances of the two multilayer coatings. As shown in Fig. 2, the predicted peak first-order efficiencies were 13% and 9% in the short and long wave bands, respectively. The peak efficiency is higher in the short band because the multilayer coating performs better at wavelengths closer to the Si *L* edge at 12.4 nm.

On the basis of the predictions of the efficiencies in the two wave bands (13% and 9%), the groove depth that was specified for the EIS grating substrate was changed from 5.8 nm to 6.0 nm. This moved the expected peak of the groove efficiency to a longer wavelength (24 nm) and increased the overall efficiency of the multilayer-coated grating in the long wave band.

The grating substrates were fabricated by Zeiss with a holographic technique to form a sinusoidal groove pattern and ion-beam etching to shape the laminar grooves and to achieve the specified groove depth (6.0 nm). The characteristics of the first three delivered grating substrates are listed in Table 1. The grooves of the FL2 grating were inadvertently patterned orthogonal to the desired orientation on the toroidal blank, and this first-delivered grating therefore served as a test grating early in the EIS grating development process. The FL7 and FL1 grating substrates in general meet the EIS instru-

Table 1. Characteristics of the Three Gratings

Characteristic	Grating Number		
	FL2	FL7	FL1
Groove frequency	4200.6 lines/mm	4201.0 lines/mm	4201.6 lines/mm
Groove depth	6.6 nm	6.7 nm	5.8 nm
Land width	105 nm	102 nm	102 nm
Land-to-period ratio	0.44	0.43	0.43
rms microroughness	0.23 nm	0.24 nm	0.22 nm
Groove side angle	35 deg	35 deg	35 deg
Groove efficiency peak	40.4% at 27.0 nm	40.7% at 28.5 nm	40.9% at 23.0 nm
Short-band -1 peak	10.4% at 19.5 nm	9.9% at 19.5 nm	12.9% at 19.5 nm
Long-band -1 peak	10.0% at 26.4 nm	9.8% at 26.3 nm	9.5% at 26.2 nm

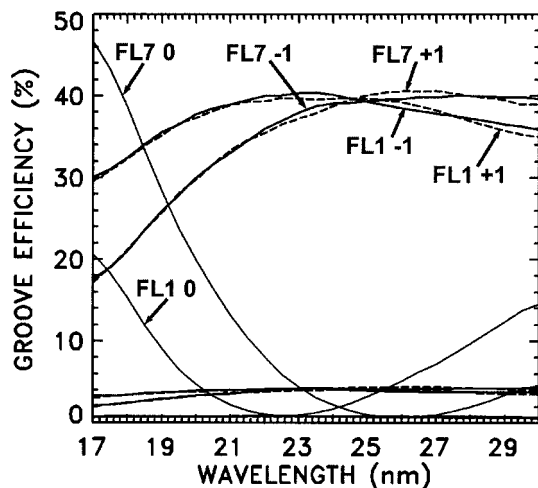


Fig. 3. Calculated groove efficiencies of the FL7 and FL1 grating substrates.

ment requirements; nevertheless the most challenging of the EIS grating specifications to achieve was the groove depth. The groove depths of the first three grating substrates, as determined by AFM studies, ranged from 5.8 to 6.7 nm compared with the EIS specified value of  $6.0 \pm 0.4$  nm.

The calculated groove efficiencies of the FL1 and FL7 gratings, with groove depths of 5.8 and 6.7 nm, are shown in Fig. 3. The groove efficiency of the FL2 grating (groove depth of 6.6 nm) is similar to FL7 and

is not shown. The FL1 grating, with a groove depth closest to the EIS specified value of 6.0 nm, has a maximum first-order groove efficiency of 41% (and minimum zero-order efficiency) in the 22–24-nm wavelength region, midway between the two EIS wave bands as desired. The FL7 grating, with a groove depth of 6.7 nm, has a maximum first-order groove efficiency (and minimum zero-order efficiency) in the 26–28-nm wavelength range, which is in the EIS long wave band. The FL7 zero-order efficiency is relatively high in the EIS short band because of the larger than optimal groove depth. For both gratings, the groove efficiencies in the higher orders ( $>1$ ) are  $<5\%$ .

The calculated efficiencies of the FL1 and FL7 gratings with the EIS baseline short and long wave-band multilayer coatings are shown in Fig. 4. The peak values of the first-order efficiencies of the multilayer gratings and the peak values of the groove efficiencies are listed in Table 1. The FL1 grating has a groove depth (5.8 nm) closest to the EIS specified value of 6.0 nm, and the calculated efficiencies are close to the EIS baseline multilayer-coated grating efficiencies (see Fig. 2) in the short and long wave bands with peak values of 12.9% and 9.5%, respectively. The FL7 grating, with deeper grooves (6.7 nm) than optimal (6.0 nm), has higher efficiency in the long band and lower efficiency in the short band compared with FL1. This tends to equalize the efficiencies in the short and long wave bands, with peak efficiencies of 9.9% and 9.8%, respectively. However, the FL7

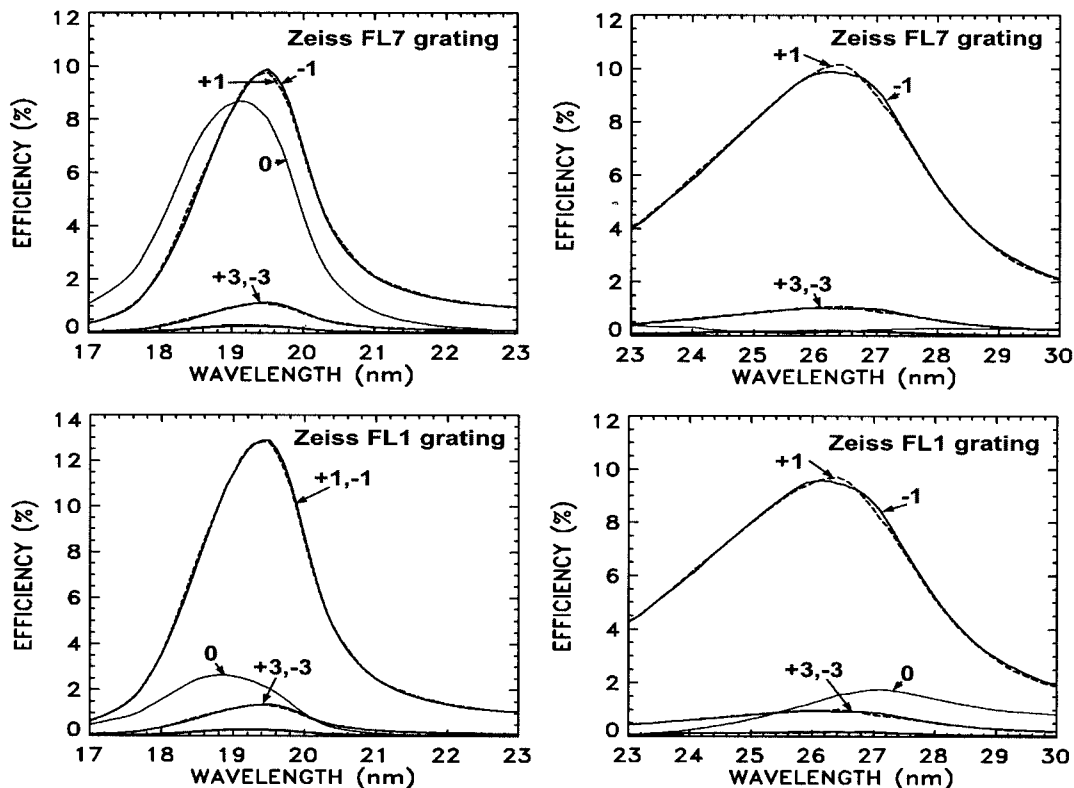


Fig. 4. Predicted efficiencies of the FL7 and FL1 multilayer-coated gratings.

peak with a  $-1$ -order groove efficiency is at 28.5 nm, near the long wavelength end of the EIS long band; and for such deep grooves, efficiency is beginning to be lost from the instrument. This is why the FL7 peak efficiencies (9.9% and 9.8%) are slightly lower than those of FL2 (10.4% and 10.0%) with a 6.6-nm groove depth. These predicted grating efficiencies illustrate the trade-offs in the efficiencies in the two EIS wave bands that primarily depend on the groove depth.

### 3. Measured Grating Efficiency and Mirror Reflectance

The FL2 grating substrate in general met the EIS instrument requirements with the exception that the grooves were not in the proper orientation on the toroidal substrate. Only the focusing properties of FL2 were affected, so the grating was considered a test grating and was characterized without a multilayer coating for the purpose of evaluating the groove profile and efficiency. The measured efficiencies were compared with the efficiencies calculated by use of the AFM groove profile and assuming a  $\text{SiO}_2$  surface. The measurements were performed at the Naval Research Laboratory beamline X24C at the National Synchrotron Light Source at Brookhaven National Laboratory. This beamline has a monochromator that passes dispersed EUV radiation to the sample chambers. The sample chambers have computer-controlled sample and detector motions. Previous measurements of Zeiss laminar gratings are described in Refs. 6 and 7.

Typical normal-incidence efficiencies for the uncoated FL2 grating, measured at wavelengths from 17.7 to 31.0 nm, are shown in Fig. 5. The efficiencies are rather low, owing to the low normal-incidence reflectance of the  $\text{SiO}_2$  surface, and increase with wavelength because of the increasing reflectance at longer wavelengths. More extensive measurements of the efficiency at a number of points on the uncoated FL2 grating, and comparisons with the calculated efficiencies, confirmed the expected wavelength dependence of the zero- and first-order efficiencies and

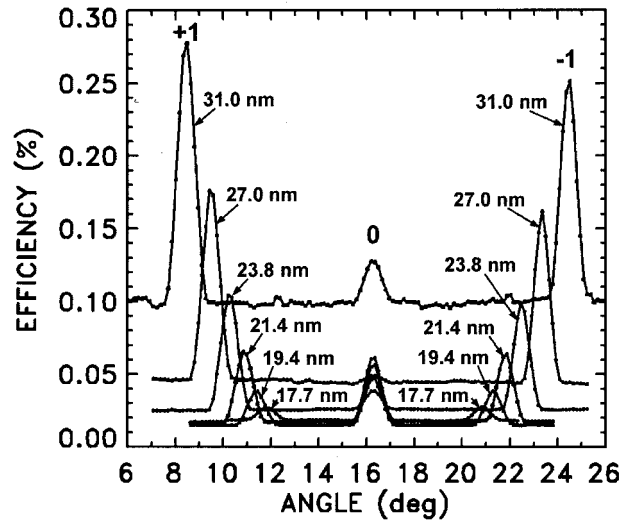


Fig. 5. Measured efficiency of the uncoated FL2 grating substrate for wavelengths from 17.7 to 31.0 nm.

the uniformity of the efficiencies across the surface of the grating.

Multilayer coatings were applied to the two halves of the first pair of flight-quality optics, the FL7 grating and the M1 parabolic mirror, at the Columbia University multilayer deposition facility. The facility capabilities are described in Refs. 8 and 9. The two multilayers with different periods, optimized to reflect the EIS short and long wave bands, were deposited onto the FL7 flight grating and the M1 flight mirror on sequential deposition runs with a mask used to cover half of the optic. The deposition parameters were optimized on the basis of the measured reflectances of small test mirrors at grazing and normal incidence. We performed subsequent tests of the mask and of the resulting coating uniformity by depositing the two EIS multilayers on sectors of full-size (100-mm- and 160-mm-diameter) spherical mirror substrates.

The reflectance of the M1 mirror was measured at

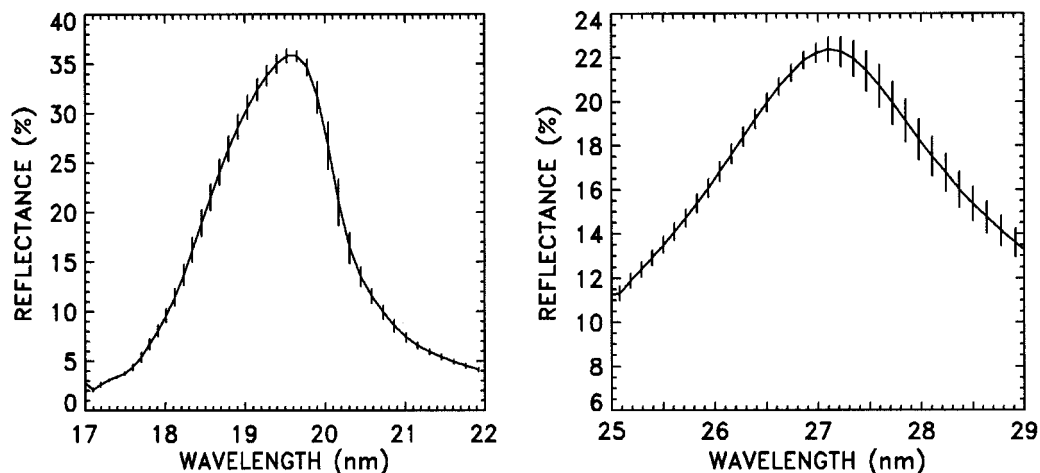


Fig. 6. Average reflectance curves measured at 39 points on the short-band side and at 39 points on the long-band side of mirror M1.

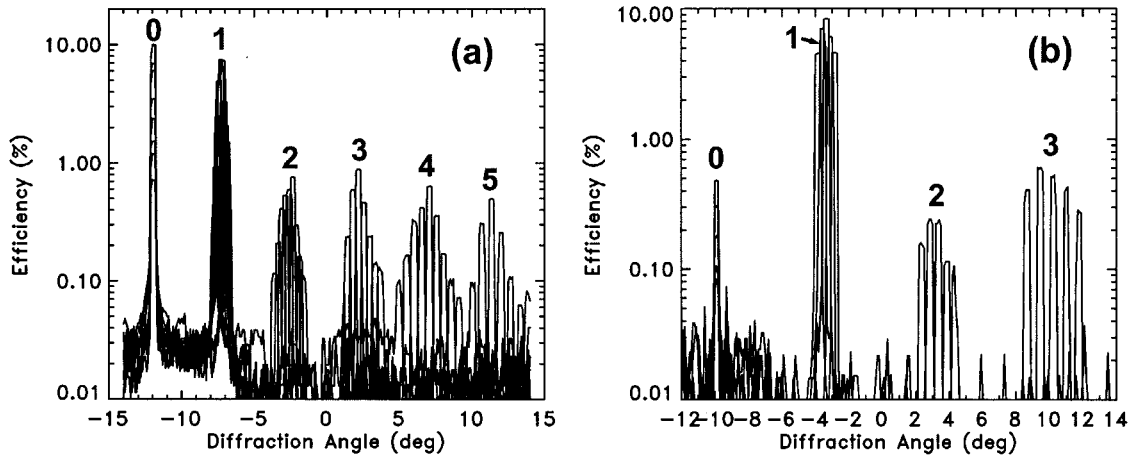


Fig. 7. Efficiency measured at (a) nine wavelengths at the central point on the short-band side of the FL7 grating and (b) five wavelengths at the central point on the long-band side.

the Naval Research Laboratory X24C beamline at 41 points on each half of the mirror (total of 82 points). The points were on a square grid with 15-mm separation and extended to the edge of the usable area (diameter of 150 mm). The angle of incidence at the center of the mirror was  $2.15^\circ$ , the same as the angle used in the EIS flight instrument. It was found that on each half of the mirror, the reflectances at the top and bottom points on the column of points closest to the mask were low, whereas the reflectances at the other 39 points were in good agreement. The low reflectance of the two extreme points on each half of the mirror is attributed to their proximity to the mask (where shadowing effects degrade the quality of the coating) and to the edge of the usable area of the mirror substrate (where the surface finish of the substrate may be degraded). The average reflectance curves of the 39 points on each half of the mirror are shown in Fig. 6, where the error bars represent the standard deviation of the 39 measurements at each wavelength. The peaks of the average reflectance curves are 35.9% at a wavelength of 19.6 nm on the short-band side and 22.4% at 27.1 nm on the long-

band side. These values are comparable to the EIS baseline peak reflectances of 32% and 23% that were used in the instrument design process.

The efficiency of the multilayer-coated FL7 grating was measured at 30 points (10 mm apart) on each side of the grating (total of 60 points). The points extended to the edge of the usable area at a diameter of 90 mm. The efficiencies were measured at nine wavelengths on the short-band side (from 17.3 to 21.3 nm) and five wavelengths on the long-band side (from 25.2 to 29.2 nm). The efficiencies measured at central points on the short-band and long-band sides are shown in Fig. 7. This illustrates the angular dispersion with wavelength, the relatively high first-order efficiencies in the two wave bands, the low higher-order efficiencies, and the low scattered light levels between the orders. The EIS spectrometer utilizes the inside first-order that appears in Fig. 7 between the zero order and the direct beam at angle zero. The angle of incidence at the center of the grating was  $6.0^\circ$ , whereas the corresponding central angle of incidence on the grating in the EIS spectrometer is  $4.48^\circ$ . The measurement angle was set to  $6.0^\circ$  to

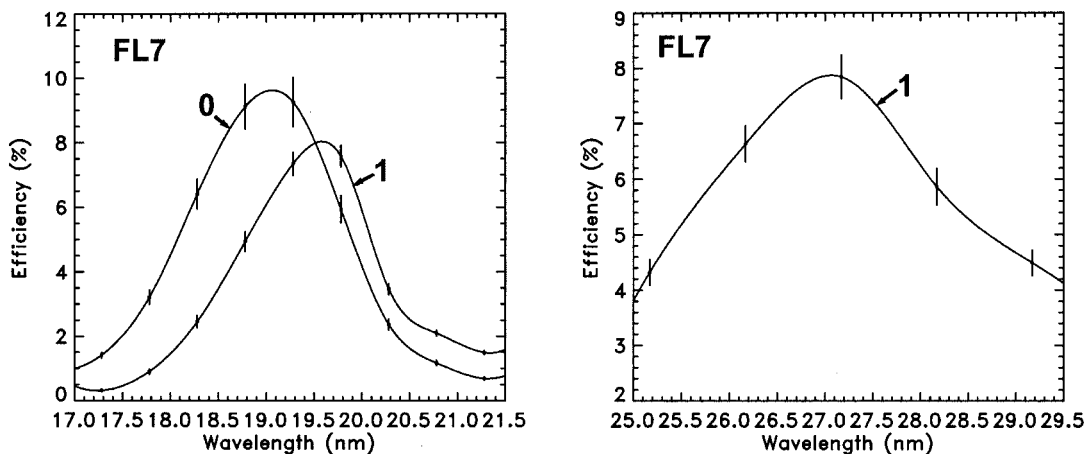


Fig. 8. Average efficiency measured at 28 points on the short-band side of the FL7 grating and at 28 points on the long-band side.

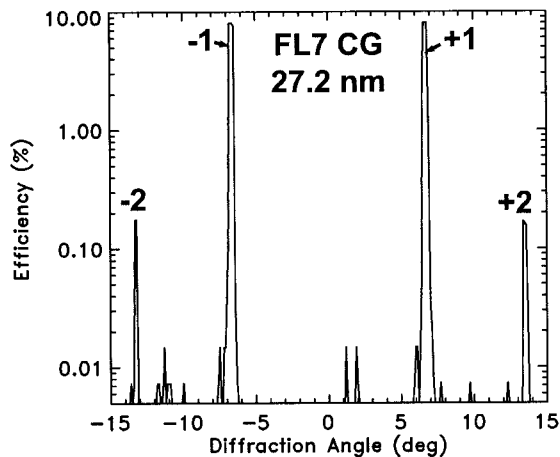


Fig. 9. Efficiency measured at exactly normal incidence at the central point (CG, center of gravity) on the long-band side of the FL7 grating and at a wavelength of 27.2 nm.

place the obscuration of the direct beam by the detector between the measured orders. Because the grating efficiency is a weak function of angle of incidence near normal incidence,<sup>3</sup> the small difference between the measurement angle ( $6.0^\circ$ ) and the operating angle ( $4.48^\circ$ ) is not significant. The angular widths of the orders in Fig. 7 are determined by the width of the detector slit, the grating-to-detector distance (70 cm), and the incident beam size (several millimeters).

The FL7 grating efficiencies measured at two extreme points near the edge of the usable area on each side of the grating were found to be low. The average efficiencies measured at the other 28 points are shown in Fig. 8. As expected based on the predicted FL7 efficiencies shown in Fig. 4, the zero-order efficiency is rather high on the short-band side of the grating because of the larger than optimal FL7 groove depth (6.7 nm in Table 1). As illustrated in Fig. 7, the zero-order efficiency on the long-band side and the higher orders

( $>1$ ) on both sides of the grating were much lower than the first-order efficiencies.

Finally, the FL7 grating was rotated so that the radiation beam was incident exactly normal to the grating surface at the central point on the long-band side, and the efficiency measured at a wavelength of 27.2 nm is shown in Fig. 9. The efficiencies measured in corresponding orders on either side of the zero-order position (which is occulted by the detector) are equal. On the basis of the efficiencies calculated at exactly normal incidence, the equality of the efficiencies in corresponding orders in either side of zero order indicate that the groove profile is symmetric about the center of the groove.

Multilayer coatings were applied to the second pair of EIS flight-quality optics, the M2 mirror and the FL1 grating, on sequential deposition runs. The mirror reflectance and grating efficiency were measured on the same grid of points as for M1 and FL7. As was the case for M1 and FL7, it was found that the reflectances and efficiencies measured at several points near the edges of the usable areas of M2 and FL1 were low. Excluding these points, the average reflectances on the short-band and long-band sides of M2 are shown in Fig. 10. The peak values are 35.2% at 19.4 nm and 21.8% at 26.7 nm, respectively; these values are comparable to the corresponding M1 values, 35.9% and 22.4%.

The efficiencies measured at the central points on the short-band and long-band sides of FL1 are shown in Fig. 11. As expected on the basis of the FL1 calculated efficiencies shown in Fig. 4, the zero-order efficiency is relatively low in both wave bands owing to the near optimal value of the FL1 groove depth, 5.8 nm in Table 1. The measured peak efficiencies in the short band and long band are 12.5% at 19.2 nm and 8.3% at 26.2 nm, respectively, and the peak efficiencies are in agreement with the corresponding calculated values of 12.9% and 9.5% listed in Table 1.

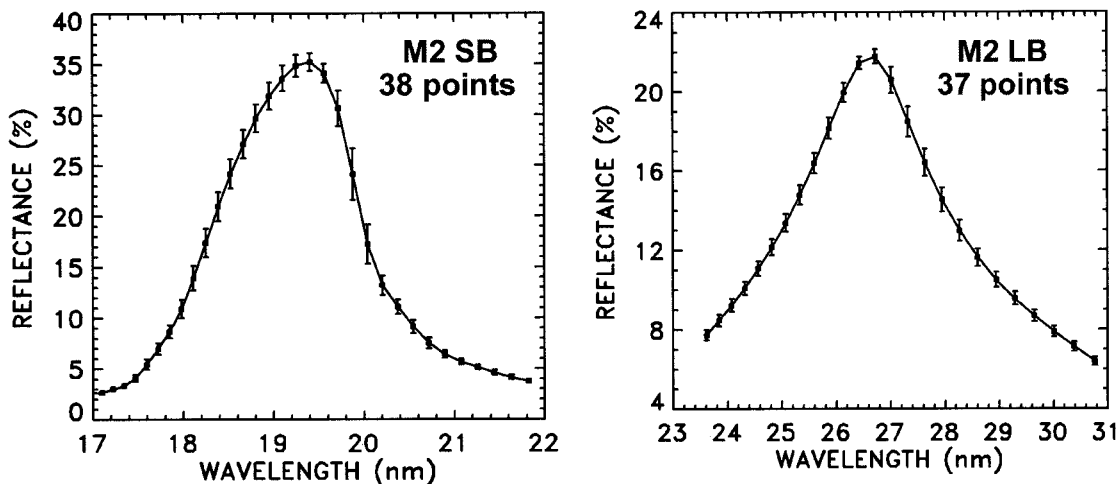


Fig. 10. Average reflectances measured on the short-band (SB) and long-band (LB) sides of M2.

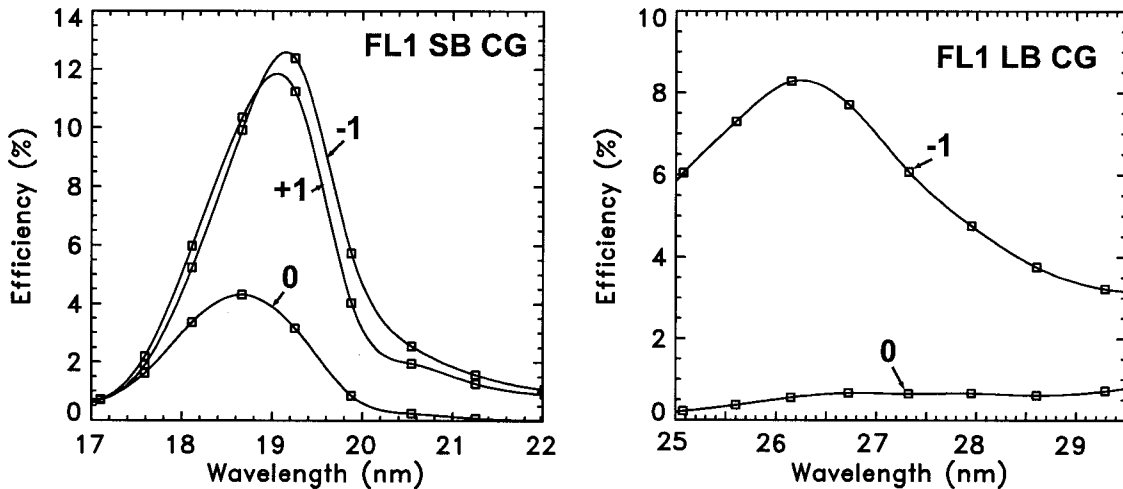


Fig. 11. Efficiencies measured at the central points (CG, center of gravity) on the short-band (SB) and long-band (LB) sides of FL1.

#### 4. Discussion

The enhancement of the normal-incidence efficiency provided by the multilayer coatings on the EIS laminar gratings is illustrated by comparison of the efficiencies of the uncoated FL2 grating (Fig. 5) and the multilayer-coated FL7 grating (Fig. 7). The application of the multilayer interference coatings results in an increase in efficiency by at least a factor of 100. This permits solar spectroscopic observations with relatively high instrument throughput and fast temporal cadence. The high-efficiency optics provide great advantages in the reduction of the instrument size, mass, and cost.

Although the measured efficiencies of the FL7 and FL1 multilayer-coated gratings are in overall agreement with the calculated values, some significant differences do occur. For example, as can be seen in Figs. 4 and 8, the FL7 zero-order efficiency measured in the short band is higher than calculated, and the measured first-order efficiency is lower than calculated. Similarly, as can be seen in Figs. 4 and 11, the FL1 zero-order efficiency measured in the short band is higher than calculated. Because the groove depth has a strong influence on the groove efficiencies, particularly the zero-order efficiency in the short band (see Fig. 3), these discrepancies can be attributed to small differences in the actual groove depth on the grating and the groove depth used in the calculations.

An additional difference between the measured and the calculated efficiencies is the wavelength separation between the first orders measured on either side of the zero order. Figure 11 indicates a small but significant wavelength separation between the two first-order efficiency curves measured on the short-band side of FL1, whereas Fig. 4 indicates no significant separation between the calculated efficiency curves. Similar trends in the wavelength separation, observed in the measured efficiencies and not in the calculated efficiencies, have occurred in previous studies of multilayer-coated gratings.<sup>1,2,6</sup>

Although the wavelength separation is small enough to be unimportant for most applications of normal-incidence multilayer gratings, the implication is that the treatment of the orders dispersed on either side of zero order in the computational model can be improved.

The relatively high efficiency of normal-incidence gratings with Mo/Si multilayer coatings, the ability to predict the performance of the multilayer gratings, and the technical capability to fabricate the gratings as designed are factors that have resulted in the implementation of a normal-incidence Mo/Si multilayer grating for the EIS instrument on the Solar-B satellite mission. Mo/Si multilayers have high reflectance at wavelengths longer than the Si *L* edge at 12.4 nm and extend to approximately 30 nm. Gratings with multilayer coatings other than Mo/Si have been demonstrated in the 9–40-nm wavelength range.<sup>1</sup> These developments permit the implementation of normal-incidence gratings covering wider wavelength and temperature ranges for high-resolution spectroscopic diagnosis of solar, astrophysical, and laboratory plasmas.

We thank Glenn Holland, William Hunter, and Michael Kowalski for assistance with the measurements. We thank the EIS instrument team for assistance with the multilayer grating design, in particular George Doschek, Clarence Korendyke, John Mariska, and Kenneth Dere. The EIS instrument development was supported by the National Aeronautics and Space Administration.

#### References

1. J. F. Seely, "Review of multilayer normal-incidence gratings operating at 9 nm–40 nm wavelengths," in *X-Ray Mirrors, Crystals, and Multilayers II*, A. Freund, A. Macrander, T. Ishikawa, and J. Wood, eds., Proc. SPIE **4782**, 224–229 (2002).
2. L. Goray and J. Seely, "Efficiencies of master, replica, and multilayer gratings for the soft x-ray–extreme ultraviolet range: modeling based on the modified integral method and comparisons with measurements," *Appl. Opt.* **41**, 1434–1445 (2002).
3. J. Seely, "Multilayer grating for the extreme ultraviolet spec-

- trometer (EIS),” in *X-Ray Optics, Instruments, and Missions IV*, R. Hoover and A. Walker, eds., Proc. SPIE **4138**, 174–181 (2000).
4. C. Korendyke, C. Brown, J. Seely, and S. Meyers, “International collaboration yields a high-performance EUV spectrometer for the Solar-B spacecraft,” *OE Mag.* **2**, 23–26 (2002).
  5. L. Goray, International Intellectual Group Inc., P.O. Box 335, Penfield, N.Y. 14526, www.pcgrate.com.
  6. J. F. Seely, M. P. Kowalski, R. G. Cruddace, K. F. Heidemann, U. Heinzmann, U. Kleineberg, K. Osterried, D. Menke, J. C. Rife, and W. R. Hunter, “Multilayer-coated laminar grating with 16% normal-incidence efficiency in the 150-Å region,” *Appl. Opt.* **36**, 8206–8213 (1997).
  7. M. P. Kowalski, T. W. Barbee, K. F. Heidemann, H. Gursky, J. C. Rife, W. R. Hunter, G. G. Fritz, and R. C. Cruddace, “Efficiency calibration of the first multilayer-coated holographic ion-etched flight grating for a sounding rocket high-resolution spectrometer,” *Appl. Opt.* **38**, 6487–6493 (1999).
  8. D. L. Windt, S. Donguy, J. Seely, B. Kjørnrattanawanich, E. Gullikson, C. Walton, L. Golub, and E. DeLuca, “EUV multilayers for solar physics,” in *Optics for EUV, X-Ray, and Gamma-Ray Astronomy*, O. Citterio and S. O’Dell, eds., Proc. SPIE **5168**, 1–11 (2003).
  9. D. L. Windt, S. Donguy, J. Seely, and B. Kjørnrattanawanich, “Experimental comparison of extreme-ultraviolet multilayers for solar physics,” *Appl. Opt.*, to be published.